Ocean Modelling 35 (2010) 206–214

Contents lists available at ScienceDirect

Ocean Modelling

journal homepage: www.elsevier.com/locate/ocemod

A variational data assimilation system for nearshore applications of SWAN

Jayaram Veeramony [a,*], David Walker [b], Larry Hsu

[a] Naval Research Lab, 1009 Balch Blvd, Stennis Space Center, MS 39529, USA
[b] SRI International, 2100 Commonwealth Blvd, Suite 210, Ann Arbor, MI 48105, USA

ARTICLE INFO

Article history:
Received 11 December 2009
Received in revised form 15 July 2010
Accepted 16 July 2010
Available online 29 July 2010

Keywords:
Data assimilation
Wave modeling

ABSTRACT

This paper uses the variational approach described by Walker (2006) for assimilation of data into the nearshore spectral wave model SWAN. The system uses observed two-dimensional spectra from the interior of the domain to correct the prescribed boundary conditions for the forward model. The objective function that determines the amount of correction to be applied is derived with the assumption that the differences between observations and model predictions are mainly a result of specification of incorrect spectra at the boundary. Using synthetic data, we show that the system reproduces the correct wave spectra at the boundary and converges to the solution with accuracy greater than 95% in only a few model iterations. Use of the assimilation system to estimate the wave field is demonstrated for Santa Rosa Island, FL. Results show excellent agreement with independent observations of the bulk (or integrated) wave parameters such as significant wave heights, peak wave periods and mean wave directions, and good agreement with observations of the two-dimensional wave spectra. The accuracy of the system is reduced when there is relatively little energy at the assimilation location or when the nonlinear processes due to wind (such as active wave growth, nonlinear transfer of energy between frequencies and directions, and breaking) are dominant in the region of interest.

Published by Elsevier Ltd.

1. Introduction

Accurate modeling of nearshore processes is critical to understanding their impact on the coastal region. Dominant processes in the nearshore are forced by the action of waves. Nearshore circulation models as well as sediment transport models use local wave energy to model the currents as well as the morphological changes in the region. Robust, sophisticated models exist for predicting the waves as well as the resulting hydrodynamics in the nearshore region. However, the accuracy of those model results depend both on the accuracy of the approximations used in the model to represent the physics and on the model inputs. For wave models in particular, one of the critical model inputs is the wave conditions at the domain boundary. In the perfect scenario, the model utilizes data that are collected at or very near the boundaries to determine these inputs. Usually, however, such data are seldom available. This dichotomy between what is generally available and what is needed for the models forms an additional significant obstacle to accurate modeling of the wave conditions in the domain.

For typical nearshore studies, the area of interest and therefore the model domain is small, say a few kilometers. In most cases, there is minimal active generation of waves by the wind in the modeled region because of limited fetch. For nearshore applications, the wave model most commonly used in conjunction with hydrodynamic models is SWAN (Ris et al., 1999; Booij et al., 1999). Modeling suites such as DELFT3D (Lesser et al., 2004) use SWAN to model the wave forcing in the entire domain, which is then used to model the currents as well as morphological changes in the nearshore. Directional resolution is important in this case because small changes in direction can lead to significant changes in the magnitude and direction of the nearshore wave-driven currents. In general, the data available in such regions are provided by directional wave buoys or similar observation systems that measure the wave energy spectrum. In this paper, we look at using such data to estimate or correct the boundary conditions such that the modeled wave conditions in the entire computational domain are improved.

Although data assimilation is relatively new for ocean wave modeling, there have been some efforts to utilize observed data in conjunction with model results to improve wave predictions. Most of these efforts have concentrated on improving wave forecasting in the open ocean, and they have been driven in part by the availability of altimeters and synthetic aperture radars (SARs) on board satellites and other airborne systems. These studies were conducted in the context of global or large-regional ocean wave modeling using the WAM wave model (Wave Model Development and Implementation, 1988; Komen et al., 1994). Initial attempts at correcting the wave field used optimal interpolation methods in

* Corresponding author. Tel.: +1 228 688 4835; fax: +1 228 688 4759.
E-mail address: jay.veeramony@nrlssc.navy.mil (J. Veeramony).

1463-5003/$ - see front matter Published by Elsevier Ltd.
doi:10.1016/j.ocemod.2010.07.008

which the observed significant wave height (and sometimes mean wave period) was used to nudge the model result towards the correct solution. Such methods correct the initial conditions provided to the model for simulations subsequent to the time the observations are collected. These methods do not account for the distribution of wave energy in the directional and frequency space. While effective in retrieving/modeling the overall energy in the vicinity of the observations, using just the bulk parameters is not enough to correct the two-dimensional spectrum. In the mid-90s, a scheme was proposed where optimal interpolation was used in conjunction with a reduced two-dimensional wave spectra (Hasselmann et al., 1997; Voorrips et al., 1997). The wave spectra is decomposed into principal wave systems where each wave system is characterized by a few integral parameters. Use of spectral information, rather than wave heights alone, was found to result in better overall prediction of wave frequency, direction, and energy in the low frequency regime (Aouf et al., 2006). Although it includes more of the observed quantities, this method only corrects the initial conditions in the model domain. Improvements to model results, although better than using only integrated parameters, were still restricted to a region around the observation location (Voorrips et al., 1997).

Relatively little has been published where both the data and wave model physics are included in the data assimilation system. In this study, we use the variational data assimilation system developed by Walker (2006) to correct the boundary conditions for SWAN given observations from the interior of the domain. The dominant processes are assumed to be shoaling and refraction; therefore, the data for assimilation needs to be outside of the surf zone. We will show that this system can provide very good results in the interior of the domain. These results include integrated parameters such as the significant wave height, peak wave period, and wave direction as well as the complete two-dimensional spectrum.

2. The assimilation system

The SWAN model (Ris et al., 1999; Booij et al., 1999) is a nearshore wave-action-balance model which can predict the evolution of the wave spectrum in coastal regions. The wave-action spectral balance is expressed as

$$\frac{\partial N}{\partial t} + \widetilde{\nabla} \cdot (\widetilde{\mathbf{C}} N) = \frac{S_{tot}}{\sigma}. \tag{1}$$

$N(\mathbf{x},\mathbf{s},t)$ is the action spectral density defined as

$$N(\mathbf{x},\mathbf{s},t) = E(\mathbf{x},\mathbf{s},t)/\sigma, \tag{2}$$

where the vectors $\mathbf{x} = (x,y)$ and $\mathbf{s} = (\sigma,\theta)$ represent spatial and spectral position respectively, E is the energy spectral density, θ is the wave direction, and the dispersion relation

$$\sigma^2 = gk \tanh kh \tag{3}$$

relates the intrinsic radian frequency σ and the wave number $k = 2\pi/\lambda$ with g representing the gravitational acceleration and h the water depth. In (1), $\widetilde{\nabla} = \left(\frac{\partial}{\partial x}, \frac{\partial}{\partial y}, \frac{\partial}{\partial \sigma}, \frac{\partial}{\partial \theta}\right)$ and $\widetilde{\mathbf{C}} = (C_x, C_y, C_\sigma, C_\theta)$ represent the wave-energy propagation velocities in physical and spectral space. The x- and y-direction components of the wave-propagation velocities are given by

$$C_x = U + C_g \cos\theta, \quad C_y = V + C_g \sin\theta, \tag{4}$$

where $U(\mathbf{x},t)$ and $V(\mathbf{x},t)$ are the x and y components of the ambient current velocities, specified as inputs to the problem, and the wave group velocity is

$$C_g = \frac{1}{2}\sqrt{\frac{g}{k}\tanh kh}\left(1 + \frac{2kh}{\sinh 2kh}\right). \tag{5}$$

The other two velocities C_σ and C_θ are energy propagation velocities in the spectral domain caused by depth and current variations. They are defined in terms of the apparent frequency Ω (as seen by a stationary observer), which includes a Doppler shift induced by the ambient current

$$\Omega = \sigma + k(U\cos\theta + V\sin\theta). \tag{6}$$

The spectral propagation velocities are given by

$$C_\sigma = \frac{\partial \Omega}{\partial t}, \quad C_\theta = \frac{1}{k}\left(\frac{\partial \Omega}{\partial x}\sin\theta + \frac{\partial \Omega}{\partial y}\cos\theta\right). \tag{7}$$

The source term S_{tot} on the right-hand side of (1) is described in detail in Ris et al. (1999) and includes the effects of wind growth (S_{in}) and energy transfer in the spectrum by nonlinear wave-wave interactions (resonant triad and quartet interactions, S_{nl}). Significant additional contributors to the source term are various processes by which wave energy is dissipated. These include white-capping ($S_{ds,w}$), bottom friction ($S_{ds,b}$) and depth-induced breaking ($S_{ds,br}$).

This set of equations can be solved for the action spectrum $N(\mathbf{x},\mathbf{s},t)$ for a domain subject to appropriate boundary conditions. For portions of the wave spectrum with propagation velocities that carry energy into the domain, the 'incident' wave spectrum must be specified on the boundary. In the spectral domain, for most practical implementations, the spectral density is required to vanish on the upper and lower frequency (σ) boundaries; this condition is satisfied by locating the σ boundary far from the energy-containing region of the spectrum. The boundary conditions in θ are that the spectrum is periodic. In addition to these boundary and initial conditions, complete specification of the mathematical problem requires the bathymetry $h(\mathbf{x})$ and current fields $U(\mathbf{x},t)$, $V(\mathbf{x},t)$ to be prescribed.

3. Assimilation methodology

In this section we present the variational data assimilation approach used. The approach was originally developed for the assimilation of synthetic aperture radar data and is described in Walker (2006). In the present study, a reduced version of the algorithm has been used for wave-spectrum data. For simplicity and compactness of presentation, we adopt a strong-constraint approach using Lagrange multipliers (e.g., LeDimet and Talagrand, 1986), but the same result can be derived by starting with a weak-constraint formulation of Bennett (1992) and then taking the strong constraint limit. The model inputs being estimated are penalized in the objective function to ensure uniqueness (Bennett and Miller, 1991). An objective function which is a positive-definite measure of the difference between a set of observations and the model predictions is defined, augmented with the SWAN model as a constraint. This objective function is minimized by adjusting the SWAN-model boundary condition.

For the purposes of this study, only stationary conditions are considered, and model inputs are the incident wave spectra along the boundaries. Also, this study concentrates on the application of this modeling system to limited area domains in the nearshore region. While spectral wave models make simplifications in the representation of nonlinear energy transfers, wave generation and dissipation, the main assumption here is that, with correct boundary conditions (as far as the model is concerned), the wave spectrum in the domain can be modeled accurately. The second assumption is that the data used to correct the boundary conditions are observations from outside the surf zone. Therefore, the errors in model results caused by inaccuracies in the representation of depth-limited breaking are not present at these locations. Hence, these forcing terms are omitted in the calculation of the objective function and consequently the adjoint model. However,

these terms are included in the forward model. The third assumption is that the error in the specified boundary spectrum is uniformly distributed along the boundary.

We wish to estimate the wave spectrum $E(\mathbf{x},\mathbf{s})$ for a region $\mathcal{R}$ that minimizes the error compared to a set of spectrum observations. The estimated spectrum will be obtained from the SWAN model (1), which serves as a 'constraint' for the minimization process. The boundary spectrum $E_b(\mathbf{s})$ used for the SWAN model is assumed spatially uniform and serves as the 'control variable' for the minimization. Here, we will first define an objective function representing the constrained minimization problem, develop the adjoint equations, and present the approach used for the overall assimilation algorithm.

The objective function J is defined as follows. For a set of M observations at spatial locations $\mathbf{x}_i$, the error variance between the predicted and observed wave spectrum E can be expressed as

$$J' = \frac{1}{M}\sum_{i=1}^{M}\int_{\mathcal{S}}\left[E(\mathbf{x}_i,\mathbf{s}) - \widehat{E}_i(\mathbf{s})\right]^2 \mathbf{ds}, \tag{8}$$

where $\widehat{E}_i$ is an observation of E at location $\mathbf{x}_i$ and the integration is over the spectral domain $\mathcal{S}$. As discussed above, the situation of interest is stationary in time and one where the errors propagate from the boundary into the domain; i.e., the effects of processes represented by the source terms on the right-hand side of (1) can be safely ignored in the adjoint model. As a result, the SWAN model can be reduced to

$$\widetilde{\nabla}\cdot(\widetilde{\mathbf{C}}N) = 0. \tag{9}$$

If we require that our wave field satisfy (9) and introduce $A(\mathbf{x},\mathbf{s})$ (the adjoint wave action spectrum) as a Lagrange multiplier, our constrained minimization problem becomes one of minimizing

$$J = \int_{\mathcal{R}}\int_{\mathcal{S}}\left\{\frac{1}{M}\sum_{i=1}^{M}(E-\widehat{E}_i)^2\delta(\mathbf{x}-\mathbf{x}_i) + A\widetilde{\nabla}\cdot(\widetilde{\mathbf{C}}N)\right\}d\mathbf{s}\,d\mathbf{x} + \phi\int_{\mathcal{S}}E_b^2\,d\mathbf{s}, \tag{10}$$

where the first term in the first integral is recognized as J' and the second term is from the 'constraint' (9). The second integral penalizes the control variable E_b and is necessary to ensure a unique solution (Bennett and Miller, 1991); $\phi > 0$ sets the relative weights of the boundary spectrum and J' in the minimization result obtained.

This objective function J as defined here is a functional of N (or equivalently E) and A. We will determine the conditions for a minimum in (10) by determining where the first variations with respect to N and A vanish. Taking the first variation with respect to A recovers the constraint Eq. (9). Prior to taking the first variation with respect to N, we recast the equation in terms of N, rearrange, and make use of the divergence theorem to get

$$\begin{aligned} J = {} & \int_{\mathcal{R}}\int_{\mathcal{S}}\left\{\frac{\sigma^2}{M}\sum_{i=1}^{M}(N-\widehat{N}_i)^2\delta(\mathbf{x}-\mathbf{x}_i) - N\widetilde{\mathbf{C}}\cdot\widetilde{\nabla}A\right\}d\mathbf{s}\,d\mathbf{x} \\ & + \int_{\mathcal{S}}\int_{\partial\mathcal{R}} NA\widetilde{\mathbf{C}}\cdot\hat{n}\,d\xi\,d\mathbf{s} + \phi\sigma^2\int_{\mathcal{S}}N_b^2\,d\mathbf{s}, \end{aligned} \tag{11}$$

where the spatial portion of the second integral is over the domain boundary $\partial\mathcal{R}$, and $\hat{\mathbf{n}}$ is a unit normal. The first variation with respect to N is

$$\begin{aligned} \delta J = {} & \int_{\mathcal{R}}\int_{\mathcal{S}}\left\{2\frac{\sigma^2}{M}\sum_{i=1}^{M}(N-\widehat{N}_i)\delta(\mathbf{x}-\mathbf{x}_i) - \widetilde{\mathbf{C}}\cdot\widetilde{\nabla}A\right\}\delta N\,d\mathbf{s}\,d\mathbf{x} \\ & + \int_{\mathcal{S}}\left\{\int_{\partial\mathcal{R}} A\widetilde{\mathbf{C}}\cdot\hat{n}\,d\xi + 2\phi\sigma^2N_b\right\}\delta N_b\,d\mathbf{s}, \end{aligned} \tag{12}$$

where the two integrals on the second line have been combined. Since δN is arbitrary, the first integral will vanish only if the balance of the integrand is identically zero, so for the minimum in J we require that

$$-\widetilde{\mathbf{C}}\cdot\widetilde{\nabla}A = -\frac{2\sigma}{M}\sum_{i=1}^{M}(E-\widehat{E}_i)\delta(\mathbf{x}-\mathbf{x}_i); \tag{13}$$

this is the governing equation for A, the adjoint wave action spectrum. The first variation of J now consists solely of

$$\delta J = \int_{\mathcal{S}}\left\{\int_{\partial\mathcal{R}} A\widetilde{\mathbf{C}}\cdot\hat{n}\,d\xi + 2\phi\sigma^2N_b\right\}\delta N_b\,d\mathbf{s}, \tag{14}$$

and so we can identify

$$\frac{\partial J}{\partial E_b} = \frac{1}{\sigma}\frac{\partial J}{\partial N_b} \sim \int_{\partial\mathcal{R}}\frac{A}{\sigma}\widetilde{\mathbf{C}}\cdot\hat{n}\,d\xi + 2\phi E_b, \tag{15}$$

which is the gradient of J with respect to the boundary spectrum. The gradient depends on the boundary spectrum E_b and the integral of the product of the adjoint spectrum A and the boundary normal component of the spatial advection velocity $\widetilde{\mathbf{C}}$ along the boundary $\partial\mathcal{R}$.

So, collecting and organizing our results, the complete set of equations for the assimilation algorithm consists of: the cost function J

$$J = \frac{1}{M}\sum_{i=1}^{M}\int_{\mathcal{S}}\left[E(\mathbf{x}_i,\mathbf{s}) - \widehat{E}_i(\mathbf{s})\right]^2 d\mathbf{s} + \phi\int_{\mathcal{S}}E_b(\mathbf{s})^2\,d\mathbf{s}, \tag{16}$$

which serves as a diagnostic, used to determine convergence; the SWAN model (1), for stationary conditions

$$\widetilde{\nabla}\cdot(\widetilde{\mathbf{C}}N) = \frac{S_{tot}}{\sigma}; \tag{17}$$

the adjoint SWAN model

$$\widetilde{\mathbf{C}}'\cdot\widetilde{\nabla}A = -\frac{2\sigma}{M}\sum_{i=1}^{M}(E-\widehat{E}_i)\delta(\mathbf{x}-\mathbf{x}_i), \tag{18}$$

where $\widetilde{\mathbf{C}}' = -\widetilde{\mathbf{C}}$; and finally, the gradient of J with respect to the boundary condition E_b

$$\frac{\partial J}{\partial E_b} = \int_{\partial\mathcal{R}}\frac{A}{\sigma}\widetilde{\mathbf{C}}\cdot\hat{n}\,d\xi + 2\phi E_b. \tag{19}$$

Eqs. (17)–(19) are the Euler–Lagrange equations, which define the minimum for J.

It should be noted that the adjoint SWAN equation was developed using a homogeneous form of the SWAN model, while in the assimilation algorithm the complete SWAN model is used for the forward modeling. If the observation locations are restricted to areas in the domain where the errors primarily arise from the propagation of errors at the boundary, not because of dissipation or generation, then it is expected that the assimilation system will be able to correct the wave field in the entire domain. In addition, using the full SWAN model for the forward model allows the full region to be calculated as accurately as possible, in particular the shallow region between the observation locations and the shoreline that includes the surf zone.

The assimilation algorithm proceeds from an initial guess for E_b (which could be zero) and calculates an estimate of the wave spectrum $E(\mathbf{x},\mathbf{s})$ using (17). The adjoint SWAN model (18) is then solved with homogeneous boundary conditions (for inward propagating waves) and with the spectrum error as the source term. The adjoint spectrum at the boundary $A(\mathbf{x},\mathbf{s})$, $\mathbf{x}\in\partial\mathcal{R}$, and $E_b(\mathbf{s})$ are then used in (19) to calculate the gradient. The gradient is used in a conjugate-gradient minimization scheme to iteratively determine the $E_b(\mathbf{s})$ which minimizes J.

4. Application of the assimilation algorithm

The assimilation system is tested off the coast of Santa Rosa Island, FL, where a study was undertaken during the latter part of January, 2009 (Edwards et al., 2009). Wave energy during this period was mild, with significant wave heights (H_s) less than 1.5 m, and the waves entered the region mostly from the southeast. Prior to the start of the experiments, the bathymetry was determined using single and multi-beam acoustic surveys. The computational domain and the bathymetry contours are shown in Fig. 1. The water depth along the offshore boundary varied from 20 to 25 m, and it decreased gradually shoreward. From the 10 m contour to the shoreline, there is very little alongshore variability in the water depths. Multiple buoys were deployed in this region during the study. These buoys recorded and transmitted measurements of directional wave energy every hour. The buoy locations in the domain are also shown in Fig. 1. The corresponding water depth at each location and the duration of operation for each buoy are given in Table 1. One of these buoys (Sentry ADCP, henceforth SAB) also recorded the current profile.

Before looking at the results using the collected data, we first look at some synthetic data sets generated by running the SWAN model. Using synthetic data allows us to evaluate the system independent of the accuracy of the SWAN model and also allows us to verify that the system can recreate the boundary conditions. To generate the data, SWAN was run for the region shown in Fig. 1. The incident wave spectrum was a Pierson–Moskowitz spectrum as given by Donelan et al. (1999),

$$E(\sigma,\theta) = \alpha g^2 (2\pi)^{-4} f^{-5} \exp\left[-1.25\left(\frac{f_m}{f}\right)^4\right] \frac{1}{2}\operatorname{sech}^2[\beta(\theta-\theta_p)], \quad (20)$$

which has the wind speed (U_{10}) and direction (θ_p) at 10 m above the ocean surface and the directional spreading (β) as the defining parameters. In the above equation, $f = 2\pi/\sigma$ is the wave frequency and we use the default values of $\alpha = 0.0081$ and $f_m = 0.13g/U_{10}$ given in Alves and Banner (2003). We use $\beta = 2$ as the value for the directional spreading factor. We show six different simulations (Table 2) ranging from little wave activity to significant wave energy in the domain, either with winds present in the domain (i.e., possibility of wave generation in the domain) or no winds in the domain (all energy coming from the boundary). Wave spectra obtained at the location of Triaxys buoy #1 (henceforth TA1) from the SWAN model run was used as input to the assimilation system. In the three cases where winds were present in the domain, a constant value of U_{10} was specified throughout the domain. Furthermore, for these cases, quadruplet interaction and dissipation due to white-capping were enabled in the forward model.

Fig. 2 shows the difference in the significant wave height between the results from the original SWAN model run and the simulation using boundary conditions given by the assimilation system for the three cases in Table 2, with and without including the effects of wind in the domain for the forward model. For the cases where the wave energy enters the domain only from the boundary (cases a, c, and e), the difference between the data and the results is less than 5% everywhere in the domain. We see some degradation in the results away from the assimilation location. The errors are largest for the case where the incoming wave energy is

Table 1
Wave buoy types, the corresponding water depths at their deployment locations and their duration of operation.

Buoy type (name)	Water depth(m)	Duration of operation
Triaxys #1 (TA1)	5.3	Jan 27, 5 pm – Jan 31, 7 pm
Sentry ADCP (SAB)	10.2	Jan 27, 3 pm – Feb 5, 9am
Triaxys #2 (TA2)	17.8	Jan 28, 1 am – Jan 29, 5 am
Sentry (SIB)	20.6	Jan 27, 2 pm – Feb 5, 9 am

Table 2
Wind speed used for generating the boundary spectrum for the different cases in the twin experiments and the resulting wave-averaged parameters. Cases (b), (d) and (f) are the same as cases (a), (c) and (e), but with the corresponding U_{10} acting in the domain as well. The mean direction was 100° (waves from the east have direction 0° and from the south have direction 90°).

Case	U_{10}(m/s)	H_{sig}(m)	Mean period T_m(s)
(a)	5	0.56	2.74
(c)	10	2.28	5.76
(e)	12	3.3	6.96

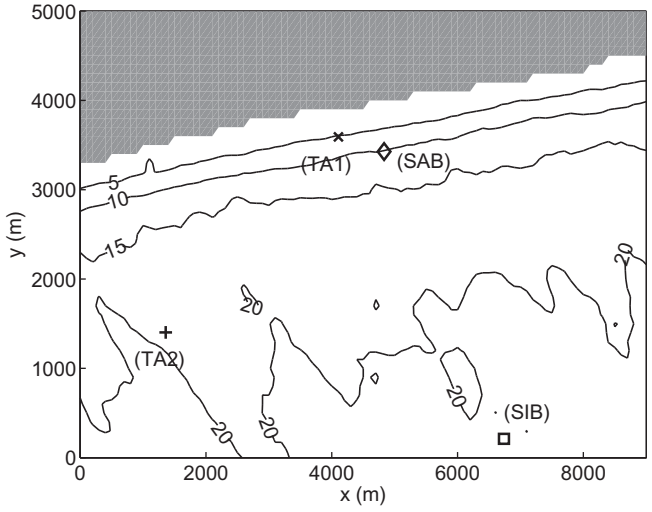

Fig. 1. Computational domain at Santa Rosa Island, FL, showing the bathymetry in the region. The locations of the buoys are also shown: Triaxys buoy 1 (×), Triaxys buoy 2 (+), Sentry ADCP buoy (◇), Sentry buoy (□).

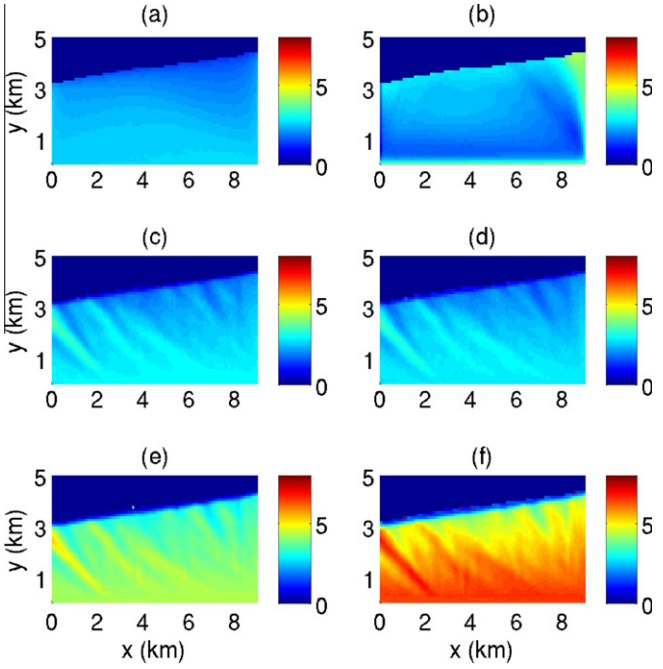

Fig. 2. Difference between the actual and the modeled significant wave height (H_{sig}) as a percentage of the actual wave height for all six cases.

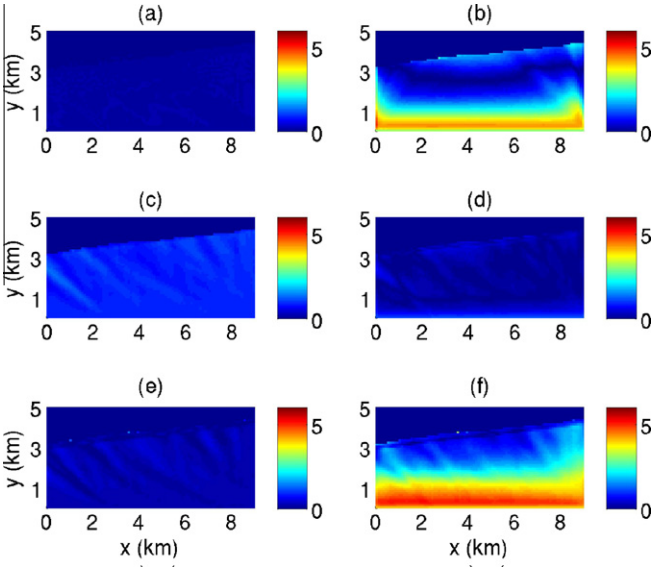

Fig. 3. Difference between the actual and the modeled mean wave period (T_m) as a percentage of the actual mean wave period for all six cases.

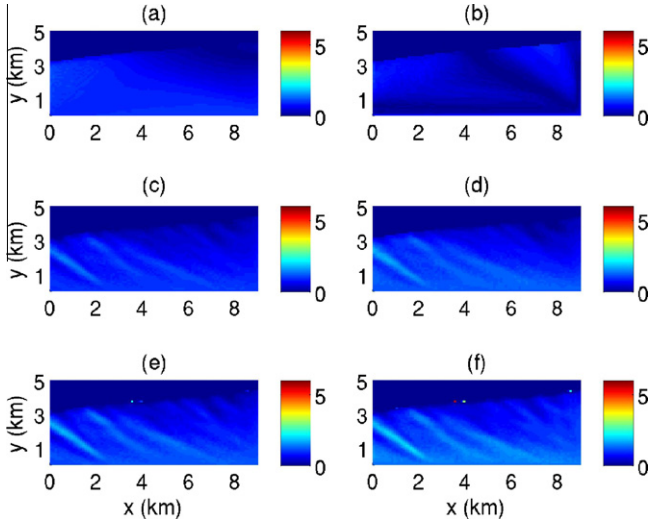

Fig. 4. Difference between the actual and the modeled mean wave direction (θ_m) as a percentage of the actual mean wave direction for all six cases.

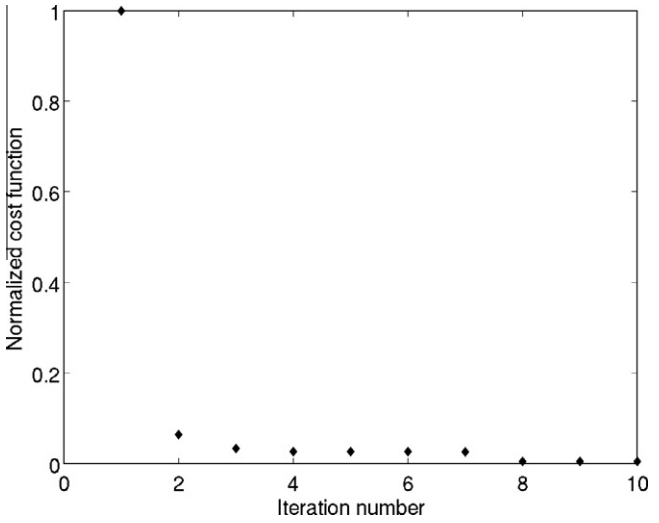

Fig. 5. The cost function as a function of the iteration number for case (f).

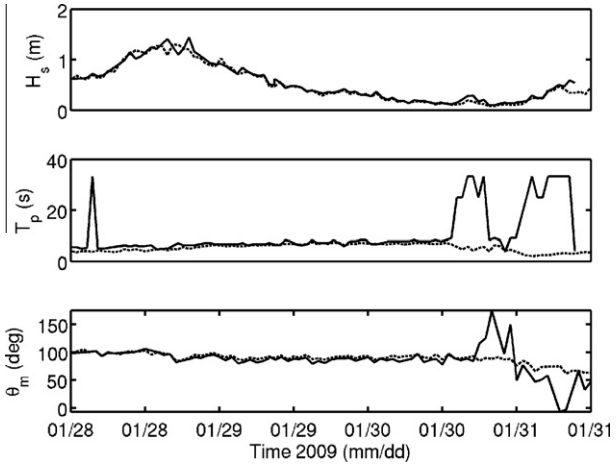

Fig. 6. Comparison of integrated parameters at the assimilation location (Triaxys buoy 1). Solid lines are data and dashed lines are model results.

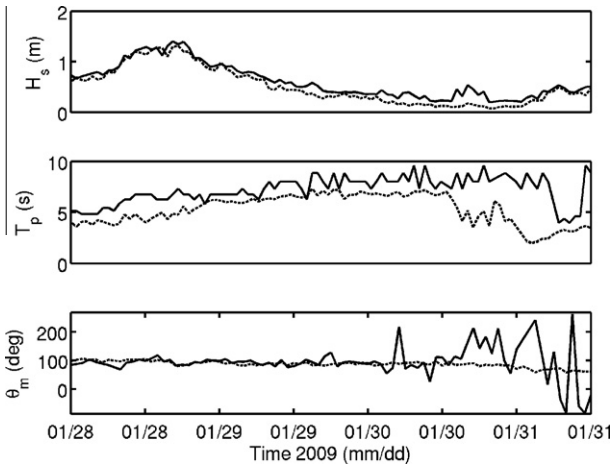

Fig. 7. Comparison of integrated parameters nearshore (Sentry ADCP buoy). Solid lines are data and dashed lines are model results.

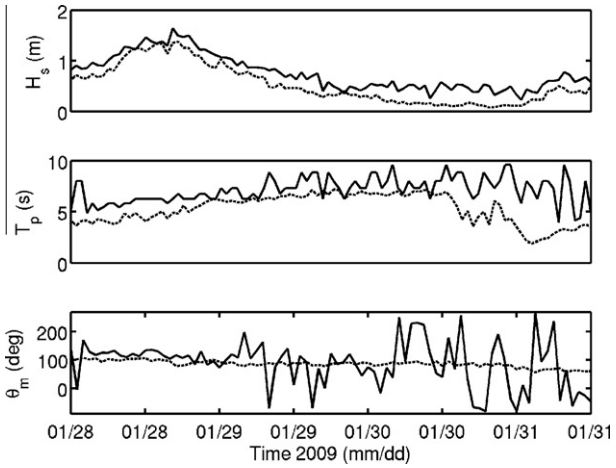

Fig. 8. Comparison of integrated parameters near the offshore boundary (Sentry buoy). Solid lines are data and dashed lines are model results.

very high. For the cases where there is wind in the domain in addition to wave energy entering the domain via the boundary, the picture is mixed. Where the incoming wave energy is small (case b), the errors are larger at the boundary (close to 4%), then decrease to near zero almost immediately, then increase to about 3% close to the assimilation location. This change in error can be directly attributed to the generation of waves in the domain. Since the data at the assimilation location have additional energy due to the wave growth in the domain, the system adjusts the energy entering the boundary to compensate for this input of energy into the waves. Thus the result of the assimilation shows a larger amount of wave energy entering the domain than is actually measured. For the case with the strongest winds (case f), white-capping and energy transfer between the frequencies are also factors. Even here, the maximum difference between the data and results from the assimilation system is less than 7% in the domain.

Fig. 3 shows the difference in the mean wave period between data and the assimilation system. Again, we see that when there is no wind in the domain, the assimilation system reproduces the original data very accurately (within 2%). When wind is present, errors are still less than 6% in the domain even for the extreme case (f). Fig. 4 shows the difference in the mean wave direction. Here we see that the results between the data and the assimilation system are nearly identical everywhere. The maximum difference is approximately 3%. Fig. 5 shows the cost function as a function of the iteration step for case (f). Each iteration involves one run of the adjoint model and one run of the forward model with the updated boundary condition. We see that most of the variance in the domain is captured in the first iteration itself. After about seven iterations, the system has reached its convergence limit.

The results shown next were obtained by using the hourly observations of the wave spectrum from TA1 to estimate the SWAN boundary condition for that time, assuming stationary conditions (Figs. 6–10). For each measurement reported by the buoy, the initial guess for boundary spectrum was zero, and the algorithm tended to converge in 10–15 iterations, or fewer. Estimated spectra obtained from SWAN are compared to spectra from the nearshore buoy SAB, and the offshore Sentry buoy (henceforth

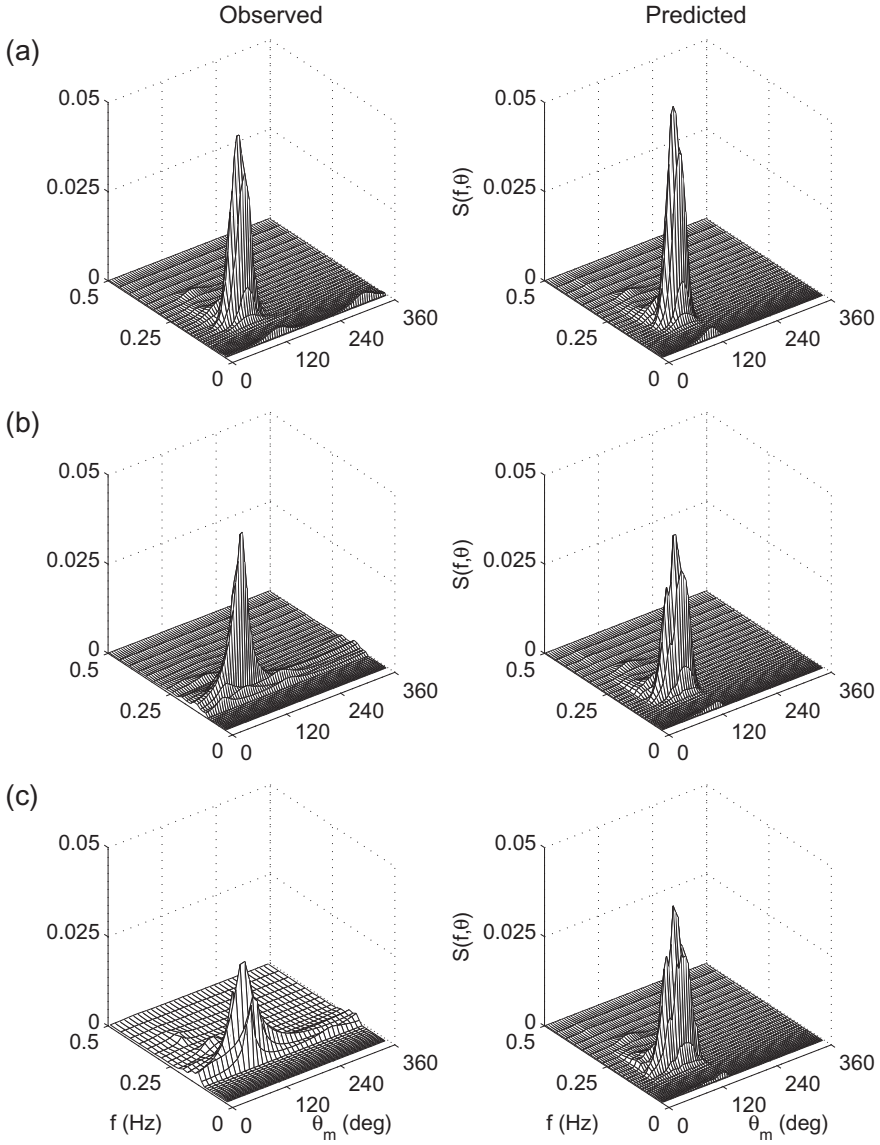

Fig. 9. Observations (left column) and predictions (right column) of wave spectral energy density ($m^2/Hz/deg$) for Jan 28, 3 pm when the difference between observations and predictions of H_s is the largest. Rows (a), (b), and (c) are at buoys TA1 (assimilation location), SAB (nearshore location) and SIB (offshore location), respectively. For waves propagating northward, $\theta_m = 90°$.

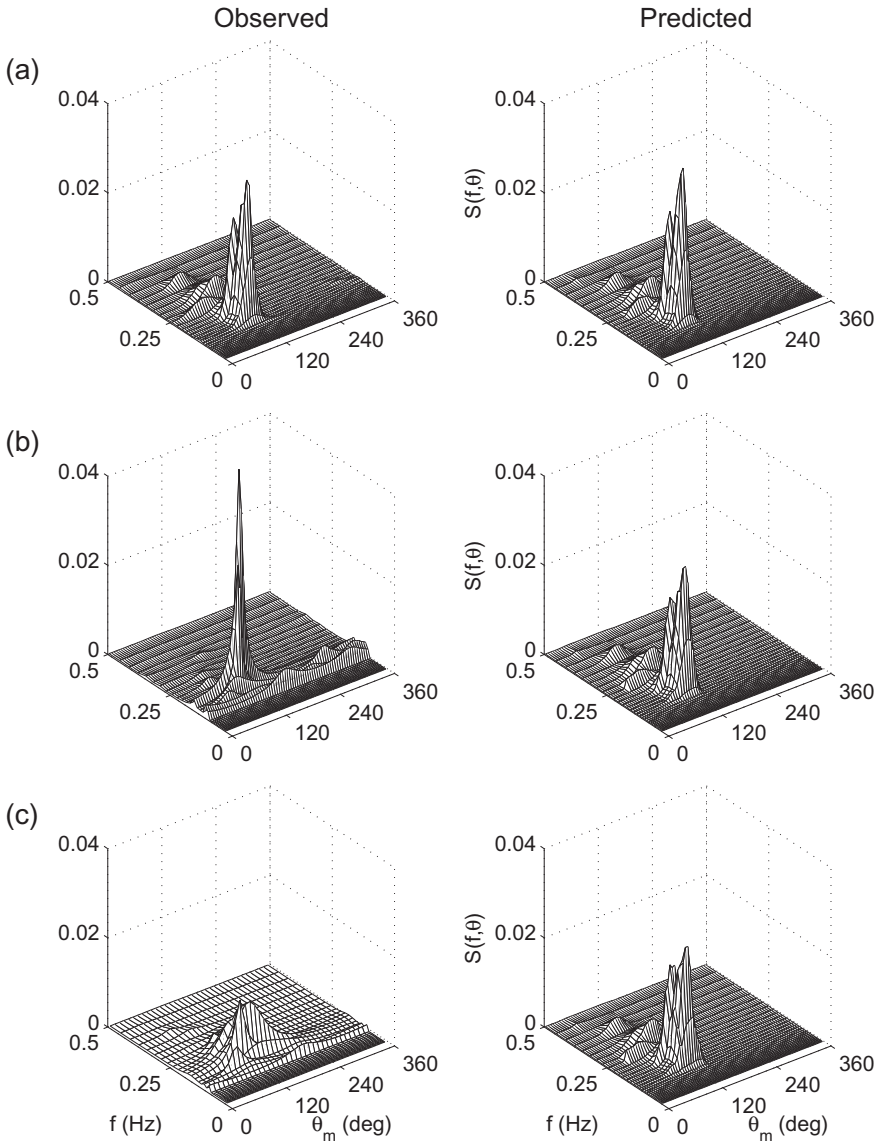

Fig. 10. Observations (left column) and predictions (right column) of wave spectral energy density ($m^2/Hz/deg$) for Jan 28, 12 pm when the difference between observations and predictions of H_s is the largest. Rows (a), (b), and (c) are at buoys TA1 (assimilation location), SAB (nearshore location) and SIB (offshore location), respectively. For waves propagating northward, $\theta_m = 90°$.

SIB). The offshore Triaxys buoy #2 (TA2) was operational for only a short time (27 observations) compared to the other locations (191 observations). The comparisons at this location were similar to those at SIB and are not shown here.

Fig. 6 compares the results of the assimilation algorithm to the observed data at the assimilation location (TA1) for the integrated parameters H_s (significant wave height), T_p (peak wave period), and θ_m (mean wave direction) for the entire observation time period. (In this figure and elsewhere, all times are UTC.) The maximum difference between observations and predictions of H_s at this location is 0.32 m, which occurred on Jan 28 at 3 pm. The minimum predicted error was approximately 0.01 m, which occurred at a number of different observation times. The mean difference between the observations and the predictions is 0.07 m. We see from the figure that the peak wave periods (T_p) are also mostly recovered. The largest errors for T_p are between 20 s and 30 s during the periods where the observations at this location indicate that T_p is between 30 and 40 s. This is obviously an error in the measurements as wave periods in this region are seldom that high. Also, as the following figures show, the wave periods observed at the other locations are $O(10\,s)$, which is typical for this region. One explanation for this error is that the energy during these periods is low and the spectra are broad-banded. Either the buoy is picking up the actual low-frequency motion in this region, or the sensor noise, which is common at low-frequencies, is corrupting the signal. If we only include data up to Jan 30, 12 pm (after which the wave energy in the domain is consistently low), the mean difference between the observed and predicted peak periods is less than 1 s. Comparison between the predicted and observed mean wave directions is also presented. These also show similar tendencies to those of the wave period. If all the data are included, the mean and maximum errors are significantly larger than if only data till Jan 30, 12 pm are included. Table 3 summarizes the errors at all three locations.

Fig. 7 shows the results at SAB, the other nearshore observation location. In general, the trend is the same as at TA1 for the difference between the observations and predictions, but average differences are slightly larger at this location. The mean difference in H_s is about 0.13 m, while the largest error of about 0.26 m is slightly lower than that observed at the assimilation location. The

Table 3
Mean and maximum differences (in parenthesis) between the estimated and observed wave parameters.

	All data			All data till January 30, 12 pm		
	$H_s(m)$	$T_p(s)$	θ_m(deg)	$H_s(m)$	T_p (s)	θ_m(deg)
TA1	0.07(0.32)	11.69(31.2)	20(82)	0.07(0.32)	0.9(2.3)	4(9)
SAB	0.13(0.26)	2.46(6.68)	53(197)	0.12(0.26)	1.45(2.8)	22(60)
SIB	0.25(0.44)	2.43(6.34)	76(212)	0.23(0.42)	1.4(3.9)	59(159)

predicted energy here is generally lower than the observed value. In addition, the mean difference in the peak period is slightly larger than at TA1, with the predictions generally lower than the observations by an average of about 2 s. This average is skewed upwards because of the larger differences during the times when the energy is very low. If the results at these times are not taken into consideration when calculating the differences, they are closer to 1.5 s on average. The wave directions also show larger errors at this location than at the assimilation location.

Fig. 8 shows the results closer to the boundary at SIB. The differences are even larger here, which is to be expected for a few reasons. First, the wind forcing and associated nonlinear interactions are omitted, although even in small areas with very benign seastates, one would expect some wave generation. Second, the effect of dissipation (other than by bottom friction) is omitted in the calculation of the objective function. Thus, to reproduce the energy at the assimilation location, smaller waves than those observed are required at the boundary, which is far away from the assimilation location. The mean difference in the significant wave heights at SIB is almost 0.20 m, nearly double that at SAB. The mean difference in the peak period is similar to that seen at SAB, but the mean directional difference is somewhat larger than that seen nearshore; it ranges from 10^o to 20^o.

Fig. 9 shows the observed two-dimensional spectra at the different buoys (left column) and those predicted at the corresponding locations (right column) on Jan 28, 3 pm when the discrepancy between the prediction and observation of H_s at the assimilation location was the largest. We notice that the spectrum at the assimilation location (top row) is very similar except that the predicted spectrum has slightly smaller directional spread than the observation. At the other nearshore location (SAB, second row), the predicted spectrum shows a smaller directional spread but broader frequency spread compared to the observations. The predicted directional and frequency spread is similar to that at the assimilation location. The main reason for this is likely the omission of nonlinear interaction in the objective function. This narrowing (or lack thereof) is more substantial at the offshore location (third row). It is interesting to note that the maximum energy at the offshore location is over-predicted, while the total energy is under-predicted, which leads to a smaller significant wave height at this location (Fig. 8).

Fig. 10 shows the comparison for Jan 28, 12 pm when the prediction and observation of H_s at the assimilation location was among the smallest. As expected, here the comparison of the spectrum at the assimilation location is excellent. But at the other nearshore location (second row) the observed spectrum is very narrow-banded, and even though there is some energy in every directional bin, the maximum energy is substantially larger than predicted. In contrast, the maximum energy is predicted to be higher at the offshore location. Again the observations show more energy in every directional bin. Thus, even if the wave heights and other averaged wave parameters are recovered by the assimilation model, it does not necessarily indicate that the energy distribution is completely captured. This shows that even when errors propagating from the boundary dominate, effects of nonlinear interactions cannot be completely ignored.

5. Conclusions

The use of a wave data assimilation system based on the adjoint technique developed by Walker (2006) is demonstrated here. The system corrects the boundary conditions so as to improve predictions of the wave energy in the entire computational domain. The adjoint model is derived using a strong constraint approach which assumes that the errors between the model and data are due solely to the incorrect specification of the boundary conditions. It is assumed that the problem is dominated by propagation, and the source terms are consequently neglected in the adjoint model. The model does extremely well in reproducing wave characteristics in the domain. Results from the twin experiments show that the assimilation system is able to reproduce most of the energy in the domain even when winds and the associated nonlinearities are significant. The integrated wave properties such as significant wave heights, peak wave periods and mean directions are well recovered, even though the iterative procedure starts out with no energy in the domain. On the other hand, some of the obvious deficiencies of the model related to the initial assumptions used in deriving the objective function appear when the entire two-dimensional spectrum is compared to observations. The transfer of energy between frequencies as the waves propagate is not captured by the model. Consequently the spectral shapes from the model are broader than the measurements. Also, if most of the energy is generated inside the domain rather than entering the domain via its boundaries (in which case the strong constraint assumption is invalidated), the model does not have the physics to capture the effects. Even with those deficiencies, the system itself is very robust and consistent. However, there are obvious areas that need improvement. Future work will address the inclusion of nonlinear effects due to interactions between wave and bathymetry, wind generation, and white capping.

Acknowledgments

This work was supported by the Office of Naval Research and through the 6.2 NRL Core Project "Data assimilation and sampling strategies for nearshore model optimization and validation", Program Element 63435N. The authors thank Kacey Edwards, David Wang and Gretchen Dawson for assistance with the buoy data and the experimental setup.

References

Alves, J.H.G.M., Banner, M.L., 2003. Revisiting the Pierson–Moskowitz asymptotic limits for fully developed wind waves. Journal of Physical Oceanography 33, 1301–1323.

Aouf, L., Lefevre, J.-M., Hauser, D., 2006. Assimilation of directional wave spectra in the wave model WAM: an impact study from synthetic observations in preparation for the SWIMSAT satellite mission. Journal of Atmospheric and Oceanic Technology 23 (3), 448–463.

Bennett, A.F., 1992. Inverse Methods in Physical Oceanography. Cambridge University Press.

Bennett, A.F., Miller, R.N., 1991. Weighting initial conditions in variational assimilation schemes. Monthly Weather Review 119 (4), 1098–1102.

Booij, N., Ris, R.C., Holthuijsen, L.H., 1999. A third-generation wave model for coastal regions 1. Model description and validation. Journal of Geophysical Research 104 (C4), 7649–7666.

Donelan, M.A., Hamilton, J., Hui, W.H., 1999. Directional spectra of wind-generated waves. Philosophical Transactions of the Royal Society of London A 315, 509–562.

Edwards, K.L., Veeramony, J., Wang, D., Holland, K.T., Hsu, L., October 2009. Sensitivity of Delft3D to input conditions, Oceans'09 MTS/IEEE Conference Proceedings.

Hasselmann, S., Lionello, P., Hasselmann, K., 1997. An optimal interpolation scheme for the assimilation of spectral wave data. Journal of Geophysical Research 102 (C7), 15823–15836.

Komen, G., Cavaleri, L., Donelan, M., Hasselmann, K., Hasselmann, S., Janssen, P.A.E.M., 1994. Dynamics and Modelling of Ocean Waves. Cambridge University Press, New York.

Le Dimet, F.X., Talagrand, O., 1986. Variational algorithms for analysis and assimilation of meteorological observations - Theoretical aspects. Tellus Series A - Dynamic Meteorology and Oceanography 38 (2), 97–110.

Ris, R.C., Holthuijsen, L.H., Booij, N., 1999. A third-generation wave model for coastal regions 2 verification. Journal of Geophysical Research 104 (C4), 7667–7681.

Lesser, G.R., Roelvink, J.A., van Kester, J.A.T.M., Stelling, G.S., 2004. Development and validation of a three-dimensional morphological model. Coastal Engineering 51 (8–9), 883–915.

Voorrips, A.C., Makin, V.K., Hasselmann, S., 1997. Assimilation of wave spectra from pitch-and-roll buoys in a north sea wave model. Journal of Geophysical Research-Oceans 102 (C3), 5829–5849.

Walker, D.T., 2006. Assimilation of sar imagery in a nearshore spectral wave model. Tech. Rep. 200236, GDAIS.

Wave Model Development and Implementation (WAMDI) Group, 1988. The WAM model – a third generation ocean wave prediction model. Journal of Physical Oceanography 15, 566–592.